The final publication is available at

https://doi.org/10.1177/1468087420980565

Novella et all.

Irina Jiménez, CMT-Motores Termicos, Universitat Politecnica de Valencia, Camino de Vera s/n, E-46022 Valencia, Spain.

irji@doctor.upv.es

In-cylinder pressure, knock, Presure resonance, TJI engines, SI engines

Acoustic characterization of combustion chambers in reciprocating engines: an application for low knocking cycles recognition

Ricardo Novella1,Benjamín Pla1, Pau Bares1 and Irina Jiménez 1

[a] "affilnum –1"CMT-Motores Termicos Universitat Politecnica de Valencia E-46022 Valencia Spain

Abstract

In this paper the acoustic response of a combustion chamber is studied by assuming different pressure field excitation. The viscous effects on the combustion chamber and the finite impedance of the walls have been modeled with a first order system, which damps the resonance oscillation created by combustion. The characterization of the acoustic response of the combustion chamber has been used to identify the source of the excitation in order to distinguish normal combustion from knock. Two engines, a conventional spark ignited (SI) and a turbulent jet ignition (TJI) engine, were used, fueled with gasoline and compressed natural gas (CNG), respectively. The pressure fluctuations in the combustion chambers are analyzed and a pattern recognition system identifies the most likely source of excitation. This new criteria for knock identification permits a more consistent differentiation between knocking and no-knocking cycles, independent on the amplitude of the phenomenon, thus allowing the improvement for knock control algorithms, specially with combustion modes which heavily excite resonance, such as turbulent jet ignition or homogeneous charge compression ignition (HCCI).

1. Introduction

Knock in spark-ignition (SI) engines is an abnormal combustion phenomenon associated with the auto ignition of a portion of the fuel-air mixture ahead of the propagating flame front [1]. The combustion process of the knocking combustion has two stages: flame propagation induced by spark ignition and end-gas auto-ignition favored by the pressure increase due to the flame front evolution. The rapid auto-ignition of the end gas heavily excites resonance and reduces the engine efficiency, produces vibration noise, and heavy knock might cause damage to the engine [2]. Knock combustion research is crucial because it determines engine durability, fuel consumption, and power density, as well as noise and emission performance [3].

In recent years many solutions had been studied in order to improve the efficiency in SI engines, one is the lean burn concept, which consist of operating the engine in lean conditions ($\lambda > 1$) [4, 5]. The main problem of lean burn concept is the higher combustion instability [6]. Combustion cycle-to-cycle variability might be reduced by increasing the ignition energy [7, 8]. In order to develop technologies that increase the ignition energy, the pre-chamber ignition concept has been studied, specifically Turbulent Jet Ignition (TJI), and has proven to be an interesting solution from the point of view of stability and indicated efficiency [9].

In TJI combustion mode, knock represents one of the main constraint to increase the engine efficiency, as it cannot be easily difference from normal combustion [10, 11], since resonance is highly excited by normal combustion. In contrast with normal TJI combustion, knock might cause low or high resonance excitation, as it depends on the quantity of end-gas burnt. The intensity of the auto ignition is random in nature, i.e. hot spots, 3D temperature distribution, or in homogeneous residual gases distribution preclude its deterministic prediction. Henceforth, engine control settings might be carefully chosen to guarantee operating conditions with no knock, and consequently lowering potential engine efficiency e.g. by retarded combustion.

One of the main control parameters in SI and TJI engines is the spark advance angle (SA) [12], since it allows to modify the combustion timing and also the knock probability. The most used spark advance control strategy consists of advancing the spark angle by an amount K_{adv} to improve engine efficiency, while retarding a higher amount K_{ret} when a knocking cycle is detected in order to avoid engine damage [13].

Many knock recognition techniques for SI can be found in literature, such as ion current signal [14], accelerometers [15, 16, 17] or in-cylinder pressure. Due to its simplicity, accelerometers measurement is largely employed in industry. However, the quality of knock recognition is often affected by the associated noise [1], being the most precise technique based on in-cylinder pressure sensors because provides reliable information on the pressure oscillations in the combustion chamber [18].

Numerous knock recognition methods for SI engines based on in-cylinder pressure have been published, some

authors computed knock recognition by quantifying the pressure oscillations [18, 19], other methods are based on heat release analysis, e.g in [20] a zero-dimensional two-zones model was developed in order to predict knock occurrence through five heat transfer coefficient correlations. Further methods use the frequency domain to obtain knock indexes, using e.g discrete Fourier transform or discrete wavelet transform [21, 22].

In [23] was shown that the recognition of weak knocking cycles would substantially improve knock control algorithms. The most extended indicator for knock recognition based on in-cylinder pressure, is the maximum amplitude pressure oscillation (MAPO) which computes the maximum absolute value of the filtered pressure signal in the resonance frequency range. Nevertheless, MAPO, and most of recognition methods used, are based on a single parameter that determines the resonance intensity in the whole cycle. A pre-selected threshold must be provided for knock recognition and if the threshold is not properly chosen, the method is unable to distinguish between combustion and auto ignition, for on-board processing and control.

In [24] the authors presents a knock recognition method which take into account the intensity of the in cylinder pressure oscillations and its angular evolution, being able to detect low-knocking cycles in SI engines. However, the method still relies in a predefined threshold. In Bares et al. [25] a new knock event definition is proposed for SI engines, the method consist in comparing the excitation of the cylinder resonance produced by auto ignition with that associated with combustion, being able to detect low-knocking cycles. But the method lacks form sufficient precision when both events have similar amplitude or are located in similar crank angle positions. This might be specially critical in new combustion modes, such as TJI combustion, which heavily excite resonance due to very fast burn rates because of the ignition system, and normal combustion can easily be confused with knock [26].

The aim of the present work is to propose a more accurate knock recognition method, hence the combustion resonance in two different engines is analyzed, SI and TJI combustion engines. A model for the combustion chamber response is presented, based on how resonance excitation occurs and how it is damped during the piston stroke. The model objective is to identify two cases, normal and knocking combustion. The model is used in conjunction with a pressure-processing algorithm, previously published by the authors [2], and determines the intensity evolution of the resonant modes in the combustion chamber. The new knock identification procedure is compared with the conventional MAPO definition by using a conventional knock control strategy to maintain knock at desirable levels.

This paper is organized as follows: next section presents the experimental set up and test performed for the two engines. Then, a resonance characterization, where resonance is analyzed for both engines and the resonance indicator is presented. After, the model used is introduced and the two cases, combustion and auto ignition, are presented, and the knock recognition method is described. Next, a comparison between the new knock recognition methodology and the traditional MAPO definition is made by using the classical knock control strategy. And finally, in Section 6 the main contribution of this work are summarized.

2. Experimental set-up

Two different engines, namely engine A and B, were used to analyze the resonance excitation during normal combustion and knock:

- Engine A: A four-stroke SI production engine was used to analyze resonance and validate the new definition proposed. The control system of the engine includes an electronic control unit (ECU), which has been bypassed with an ETAS ES910 system for modifying the standard calibration. A prototyping system from National Instruments was used for acquisition, control, and diagnosis purposes.

- Engine B: A single-cylinder research version of a 4-stroke turbocharged TJI engine was used to identify the resonance excitation in such combustion mode. A prototyping system from National Instruments was used for acquisition, control, and diagnosis purposes.

The experimental data was used for illustration purposes and for experimental validations. Engine A and B specifications are shown in table 1, acquisition and control system specifications for both engines are shown in table 2, and a general control scheme is shown in figure 1.

Table 1: Engine A and B specifications

	$Engine A$	$Engine B$
Displaced volume	1300 cc	404 cc
Stroke	81.2 mm	80.5 mm
Bore	72 mm	80 mm
Compression ratio	10.6:1	13:4:1
Combustion	SI	SI-TJI
Number of cylinders	4	1
Fuel injection system	GDI	PFI

3. Resonance characterization

The frequency evolution of the in-cylinder pressure resonance in a cylindrical combustion chamber was studied in

Table 2: Engine A and B acquisition and control specifications

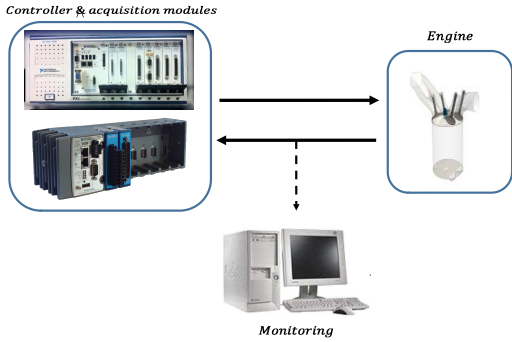|	*EngineA*	*EngineB*
Pressure sensors	AVL ZI33	Kstler 6061B
Amplifier	Kistler 5011	Kistler 5018
Controller	PXI 8110	PXI cRIO 9024(FPGA) and PXIe8133
Acquisition modules	PXI 6123 and PXI-6251	PXI 9133 and PXI 6356
Control modules	PXI-7813	NI 9758, NI 9759 and NI 9401
CAN interface module	PXI-8513	-
Sampling accuracy [CAD]	0.2	0.5

Figure 1: General scheme control of engine A and B.

[27], showing that the characteristic frequency generated in the combustion chamber can be expressed as:

$$f_{(i,j)} = a_s \sqrt{(\frac{B_{(i,j)}}{\pi D})^2 + (\frac{g}{2h})^2} \qquad (1)$$

where the axial modes g are neglected near the TDC because the height is too low ($h < D$), D is the bore of the cylinder, a_s the speed of sound and $B_{(i,j)}$ are the Bessel constants related with the radial modes, i and j represent the number of circumferential pressure modes and number of radial pressure modes, respectively [28]. The speed of sound can be calculated by measuring the trapped mass m, the in-cylinder pressure p, and estimating the instantaneous volume of the chamber V.

$$a_s = \sqrt{\frac{\gamma p V}{m}} \qquad (2)$$

where γ is the specific heat capacities ratio of the gases inside the cylinder, which can be approximated by dividing the gas mixture in three species, namely air, fuel, and burnt products, and modeled by polynomial expressions for the in-cylinder temperature such as suggested in [29].

Drapers equation is the main indicator for locating the knocking frequencies [30]. In the cases of engine A and B described above, the most significant resonant frequencies vibrate between 5 kHz and 20 kHz.

Note that Equation drap provides only the resonance frequency, but not the amplitude of such oscillation. The amplitude of the pressure fluctuations depends on how combustion excites the acoustic field, and because of the finite impedance of the walls and the viscous effects, the oscillation is damped during the piston motion.

However, is not trivial to determine the resonance intensity evolution. On the one hand, the analysis in the time domain does not provide direct information about resonance frequencies, but on the other hand, the frequency analysis with a Fourier transform does not have crank angle resolution. In order to differentiate these two phenomena time-frequency analysis, such as short Fourier transform (STFT), is required. The STFT provides the intensity of the signal in the frequency domain at each crank angle position by windowing the pressure signal and sliding the window along different crank angle position. However, high resolution in time and in frequency is not possible, i.e. for an adequate frequency analysis large windows are needed while such windows include frequency components of the surrounding and henceforth reduce the time resolution by filtering the estimation in time.

In this section STFT is used to analyzed the resonance evolution for knocking and no knocking cycles.

3.1. Knock and no-knock events

Figure 2 analyses the pressure signal for two cycles: a no-knocking (left plot) and low-knocking cycles (right plot), for both engines, top plot engine A and bottom plot engine B. The resonance intensities no-knocking and low-knocking cycles are similar for a given engine, i.e. 0.25 bar for Engine A and 1.25 bar for Engine B. The heat release, CA50 and CA90 are shown, and the corresponding frequency spectograms (STFT) by using a Blackman-Harris window of 30 CAD are also included.

Despite similar amplitudes, in knocking events an abnormal increase in the heat release rate at the end of the conventional combustion is observed. This rapid combustion produced by auto ignition excites the resonance frequencies near the end of combustion. On the other hand, for no-knocking cases frequencies are excited near the max-
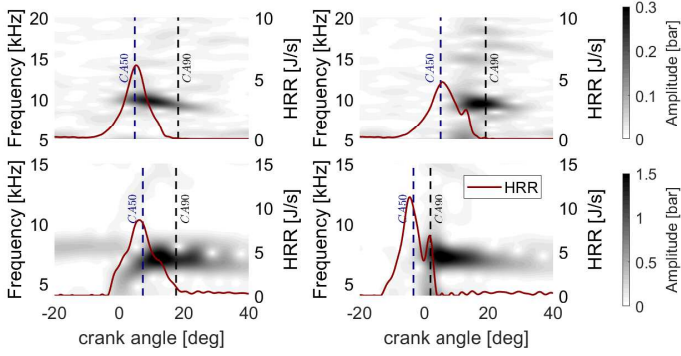
Figure 2: Top plot: Engine A. Bottom plot: Engine B. HRR, CA50, CA90 and their spectrogram from two cycles: no-knocking cycle (left) and low-knocking cycle (right). Operation point engine A: 2000 rpm. $P_{int} = 1$ bar. Operation point engine B: 2000 rpm. P_{int} = 0.75 bar.
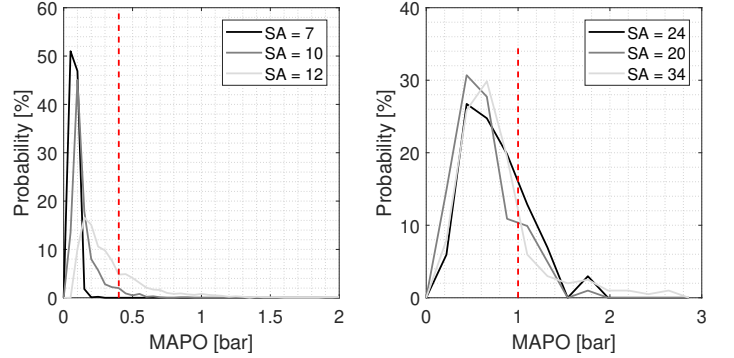

Figure 3: MAPO probability distributions over different SA. Left plot: Engine A, operation point 2000 RPM. $P_{int} = 1$ bar. Right plot: Engine B, operation point 2500 RPM. $P_{int} = 1.8$ bar.

imum of the heat release.

Note that in both cases, i.e. no-knock and knock, the MAPO amplitude, shown in figure 4 (0.3 bar for engine A and 1 bar for engine B), is similar. Therefore, if a low MAPO threshold is applied, the normal combustion would be wrongly processed as knock. On the other hand, if a high MAPO threshold is chosen, low knocking cycles will not be detected leading to dangerous knocking operating conditions.

With the aim of compare the SI and TJI combustions, MAPO probability distributions over 200 cycles for three settings of SA at each engine are shown in figure 3: the left plot shows results in Engine A while right plot shows results in Engine B. It must be noted that the resonance levels are much higher on the JTI combustion (Engine B), where conventional combustion commonly achieves 0.8 bar of MAPO. It can be also noted that, in Engine A, as SA is advanced, the MAPO distribution tends to higher values, because of knocking events, while in engine B as the SA progresses there is little change in the distribution of MAPO, as combustion hides knock and only knocking events above 1 bar are identified with MAPO criteria. In red dash line, the MAPO threshold for both engines is shown, for engine A a MAPO threshold of 0.4 bar is chosen, while for engine B a MAPO threshold of 1 bar is chosen, if a lower limit is chosen normal combustion cycles will be identify as knock.

3.2. Resonance analysis

The STFT could be used to analyze the resonance intensity by integration of the frequency spectrum in the range of the mode under analysis [31]. The first resonance frequency mode (1,0), contains most of the oscillating pressure energy [32], and is damped in a slower way due to the more intense attenuation of higher frequency modes[33]. The integration of the pressure oscillation energy over the entire frequency domain of 5–15 kHz would be sufficient

for analyzing such mode. However, the integration in the frequency domain at each crank angle position after processing a STFT has a disadvantages in real-time knock recognition applications as the computation burden of the integration calculation might be too heavy [33].

An alternative to the Fourier transform was developed in [34]. The authors suggest a modified Fourier transform to contemplate resonance theory by using a convolution with harmonics that are based on the resonance theory. These harmonics are characterized by virtual trapped masses which determine the frequency shape, in contrast to Fourier transform which uses constant frequency harmonics. The method was though to identify the most likely trapped mass, by processing the pressure signal oscillations. However, in [2] a similar alternative to the STFT was proposed. If the trapped mass is known, the convolution of that harmonic with the filtered pressure signal represents the similitude of the measured oscillation with the theoretical response of resonance. Henceforth, if the pressure signal is windowed, and the intensity of the resonance is measured at each crank angle position, an indicator of the resonance excitation evolution is provided. The discrete form is defined by:

$$I_r(\alpha) = \sum_{\alpha=\alpha_1}^{\alpha=\alpha_2} w(\alpha-\alpha_1)p_{hp}(\alpha)e^{-2\pi \sum_{\psi=0}^{\psi=\alpha} \frac{B\sqrt{\gamma(\psi)p(\psi)V(\psi)}}{\pi D \sqrt{m}}} T_s(\alpha) \quad (3)$$

where α_1 and α_2 define the interval where the resonance analysis is performed, w is a window function of $\alpha_2 - \alpha_1$ length, p_{hp} the high pass filtered pressure, and $T_s(\alpha)$ is the sampling period, which is constant only in time-based acquisition or if the instantaneous engine speed fluctuations are negligible, B is the Bessel constant, D is the bore of the cylinder, V the chamber volume, m the trapped mass, and p the in-cylinder pressure.

In a similar way than for the STFT, the use of a window function to provide crank angle resolution influences the frequency analysis. For this work a Blackman-Harris of 26 CAD was chosen: an smaller window leads to a

5

noise measurement while a larger window dilutes the frequency content in the time domain (or crank angle domain). More information about the window influence on the time-frequency analysis is provided in Appendix.

In figure 4 the pressure signal, high-pass filtering, is shown together with the evolution of the resonance indicator, which has been normalized for illustration purposes. Two cases, a no-knocking cycle (left) and a low knocking cycle (right) have been analyzed and the CA50 and the CA90 have been also represented with vertical dashed lines. The top plots correspond to Engine A and the bottom plots to Engine B.
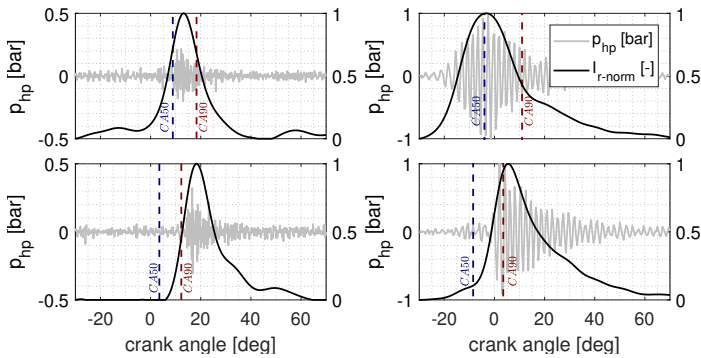

Figure 4: Resonance indicator. Left side: Engine A. Right side: Engine B. Top plots: No-knocking cycle. Bottom plots: Knocking cycle.

Analyzing figure 4, note that the maximum of I_r depends on how the combustion is exited: in no-knocking cycles (left) resonance is exited during the combustion and reaches the maximum between the CA50 and CA90, while in knocking cycles, although resonance is also excited by normal combustion, the main resonance contribution comes from the auto ignition of the end-gas, at the CA90, and hence, its maximum is found after the end of combustion.

Moreover, for knocking cycles the resonance is heavily exited after the end of combustion, and slowly damped during the expansion stroke. In no-knocking cycles, the resonance is exited during the whole combustion, around CA50.

4. Model Description and knock recognition method

4.1. Model description

In order to model the resonance evolution during normal and knocking combustion, an approximation of the resonance attenuation is analyzed. An approximation to real frequency attenuation in ducts is performed in [35], where the viscous effect in the attenuation of resonance have been analyzed, leading to an attenuation constant

which is function of the oscillation frequency and the conditions of the gases. However, Munjal studied the propagation of the wave along large ducts and did not consider the real impedance of the walls, i.e. a perfect reflection was assumed.

In this work an attenuation constant β is used to represent the movement of the piston and the real acoustical response of the combustion chamber: the finite impedance of the walls, and the viscous attenuation of the medium. The value of β is assumed to be constant for a given cycle, but might change when varying the operating conditions. The amplitude of the pressure oscillation is modeled as a first order system, which can be described in the discrete time domain as [36]:

$$G_d[z] = \frac{z}{z - e^{\beta T_s}} = \frac{1}{1 - k_d z^{-1}} \tag{4}$$

where z^{-1} represents a unit delay, $k_d = e^{\beta T_s}$ is the parameter that characterize the damping in the discrete domain, and T_s is the sampling period.

The transfer function in equation dec leads to compute the evolution of the resonance amplitude from the excitation of resonance $u(z)$:

$$A(z) = G_d[z]u(z) \tag{5}$$

However, as previously mentioned, it is not possible to identify the amplitude of the resonant mode in a concrete time step, but a diluted estimation after a window is applied. Henceforth, we can assume that the estimation provided by trans is proportional to the amplitude of the oscillation at such frequency within a time window.

$$I_r(z) \propto W[z]A(z) \tag{6}$$

where the window function $W[z]$ consists in a zero-phase filter with a Blackman-Harris window weighing:

$$W[z] = \sum_{n=-N/2}^{N/2} w_n z^n \tag{7}$$

where N is the window length in samples, and w_n the window factors that accomplish $\sum w_n = 1$.

Although the real amplitude is expected to be $A(z)$, the valuable information comes from $W[w]A(z)$ as it is comparable with the measured resonance intensity $I_r(z)$. Figure 5 shows an scheme of the model developed. The only missing information is $u(z)$, i.e. how combustion excites resonance, which should can be modeled as a function of the combustion parameters.
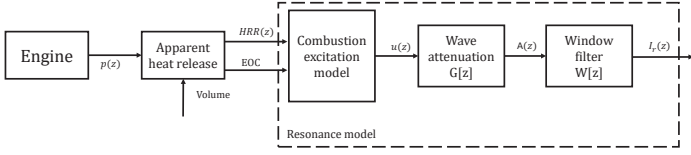
Here two hypothesis are made:

Figure 5: Resonance model scheme.

- In normal combustion the resonance excitation (u_C) is assumed to be caused by the heat fluctuations so the heat release rate (HRR) was assumed to be proportional to the resonance excitation. That means that the highest excitation is caused at the maximum HRR but all the combustion has certain contribution to the final resonance evolution.

$$u_C(z) = C \cdot HRR(z) \quad (8)$$

- In a knock event, all the excitation, is assumed to be delivered in a small step located just after the end of combustion (EOC). The intensity of the fluctuations caused is proportional to the fuel burnt in auto ignition conditions, which cannot be measured online. To represent the rapid pressure rise in auto ignition event, a step function of 0.5 CAD of a intensity $|u_A|$ has been used.

The attenuation, k_d, and the proportional relation between the HRR and the resonance excitation, C, might slightly depend on the operating conditions, but its value is expected to be almost constant and can be identified on-line.

Note that if only the shape of the resonance intensity evolution is considered by dividing by the maximum resonance intensity, C and $|u_A|$ are not required, as they only scale the model output. Henceforth, only by applying the aforementioned assumptions, and with k_d, it is possible to obtain an expected non-dimensional evolution of the resonance intensity, for both types of excitation: normal combustion or knock. Figure 6 shows the expected resonance excitation from a normal combustion event ($I_{c-model}$) and from an auto ignition event ($I_{a-model}$), and they are plotted together with the resonance indicator I_{r-norm} for the cycles shown in Figure 4.

As can be seen in figure 6, the estimated resonance evolution, I_{r-norm}, looks closer to the combustion model, $I_{c-model}$, in no knocking conditions, while it seems more correlated with the auto ignition model, $I_{a-model}$, when a knock event occurs. Note that the previous correlations to normal combustion and auto ignition models have been taken regardless of the amplitude of the resonance, which highlights the possibility of using such methodology for cycles where the resonance intensity of the combustion is similar to that from the auto ignition, i.e. either in low-knocking cycles in SI engines where the auto ignition excitation is small or in new combustion modes where
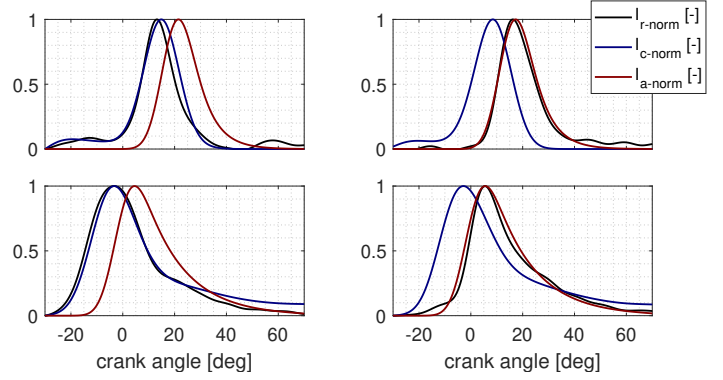

Figure 6: Combustion and auto ignition model compared with I_r for cases of figure 4.

combustion noise can create pressure oscillations with an amplitude higher than 1 bar.

The final algorithm makes use of cycle-to-cycle data processing to update the damping and combustion excitation by using an infinite input response (IIR) filter, following:

$$
\begin{align}
k_d^{k+1} &= k_d^k \alpha_{up} + \widehat{k}_d^k (1 - \alpha_{up}) \quad (9) \\
C^{k+1} &= C^k \alpha_{up} + \widehat{C}^k (1 - \alpha_{up}) \quad (10)
\end{align}
$$

where $\widehat{k}_d$ and $\widehat{C}$ are the identified damping and combustion excitation parameters, and α_{up} is the IIR filter coefficient weighting the impact of previous value (labeled with super index k) and innovation.

4.2. Knock recognition procedure

In a given operating condition, the resonance excitation due to combustion is expected to be:

$$I_c(z) = W[z]G_d[z]u_C(z) \quad (11)$$

where the combustion excitation is assumed to be proportional to the HRR, i.e. $u_C(z) = C \cdot HRR(z)$.

However, even if C is properly updated, there is certain variability due to the hypothesis taken and measurement uncertainties. In this work, all the variability is attributed to C, assuming that its expected value follows a Gaussian probability distribution $N(\overline{C}, \sigma(C))$, being $\overline{C}$ the parameter updated and $\sigma(C)$ the variability measured cycle-by-cycle.

Henceforth, the expected value of the resonance excitation is comprised between the value obtained with $\overline{C} - 3\sigma(C)$ and $\overline{C} + 3\sigma(C)$, which can be represented by I_c^- and I_c^+.

In order to allow a fast recognition of severe knock, where the resonance amplitude is high, I^+ is used as minimum threshold for severe knock. If the maximum intensity measured is higher than the maximum intensity expected:

$$\max(I_r^k) > \max(I_c^k)^+ \tag{12}$$

a severe knock event is identified. However, when the measured maximum intensity lies in the uncertainty region, the shape of the oscillation might give an insight about how resonance was initiated.

In order to identify a knock event in such cases, the estimated resonance evolution is normalized and it is compared with the combustion model and with the auto ignition model (both normalized). Although a more sophisticated pattern recognition algorithm might be developed, an euclidean distance thought the crank angle (θ) is proposed as error metric:

$$Ec(\theta_1 : \theta_2) = \sum_{\theta=\theta_1}^{\theta=\theta_2} \|I_{c-norm}(\theta) - I_{r-norm}(\theta)\| \\ Ea(\theta_1 : \theta_2) = \sum_{\theta=\theta_1}^{\theta=\theta_2} \|I_{a-norm}(\theta) - I_{r-norm}(\theta)\| \tag{13}$$

The interval $\theta_1 : \theta_2$ corresponds to the main part of the combustion process, before $CA10$ and after $CA90$, for this work a window between -30 CAD and 80 CAD is considered.

If the model match better with the auto ignition model, $E_a(\theta_2) < E_c(\theta_2)$, knock is assumed, otherwise, it is estimated that combustion is normal. Figure 7 illustrate the scheme used for knock recognition.
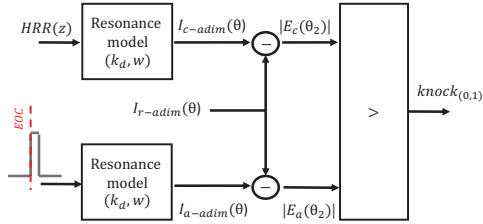

Figure 7: Scheme of the shape criteria procedure for knock recognition.

The final procedure comprise a double criteria for knock recognition and an adaptation of the main parameters for the acoustical response of the chamber: the resonance damping is continuously updated while the combustion excitation can only be updated when no knock is detected. Figure 8 resumes the entire procedure.

5. Results and discussion

5.1. Adaptation of model parameters

Figure 9 shows an histogram with the identified time constants for 500 cycles at no-knocking conditions for en-
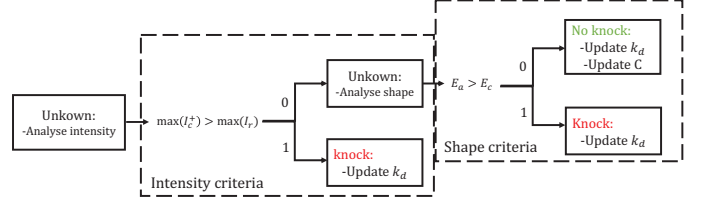

Figure 8: Scheme of the complete procedure.

gine A and B, while Figure 10 plots the proportional relation found between the HRR and the resonance intensity (I_r). Engine A was operated at 2000 rpm an exhibit an average MAPO of 0.18 bar, while Engine B was working at 2500 rpm with an average MAPO of 0.48 bar. The mean value and the standard deviation of both analysis have been collected in table 3. The characteristic time constant of both engines is 0.80 and 0.93 ms respectively, and is derived from:

$$\tau = \frac{1}{\beta} = \frac{T_s}{ln(k_d)} \tag{14}$$
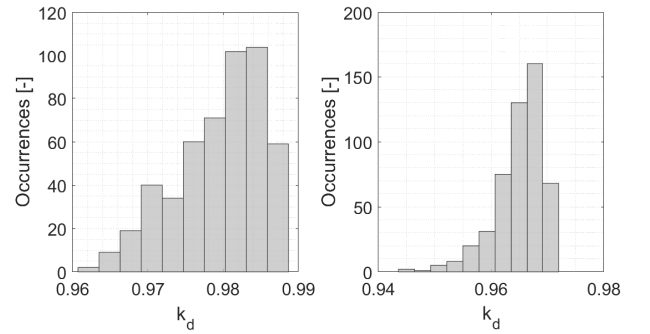

Figure 9: Damping identified at 500 cycles with conventional combustion. Left plot: Engine A. Right plot: Engine B.
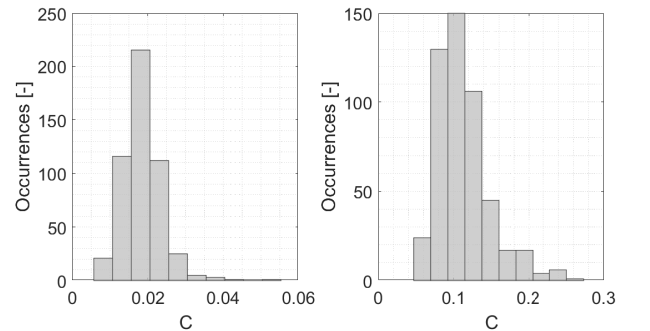

Figure 10: Proportional relation between HRR and resonance intensity identified at 500 cycles with conventional combustion. Left plot: Engine A. Right plot: Engine B.

It must be noticed that the shape of both histograms is not symmetrical, and has a small cue at lower values of damping and higher values of the combustion excitation.

That deviation from the expected value can be attributed to outliers where the resonance is not completely explained by combustion but other sources might have interfered, such as noise or an small auto ignition at the end of the combustion. Also note that the variability at damping can be neglected, i.e. represents a 0.6 % in Engine A and a 0.4 % in Engine B, but the combustion excitation variance ($\frac{\sigma(C)}{C}$) is estimated around a 30 %, so the criteria of the shape is crucial for a proper knock diagnosis.

Table 3: Model parameters

	Engine A	Engine B
$\bar{k}_d$	0.9795	0.9651
$\sigma(k_d)$	0.0059	0.0043
$\bar{C}$	0.0184	0.1125
$\sigma(C)$	0.0051	0.0352

In order to evaluate the model under transient conditions, a SA and throttle valve (X_{th}) transient was performed in engine B with the engine running at 2500 rpm. Figure 11 shows the evolution of the model parameters during the transient, the damping (k_d) and the combustion excitation (C) characteristics have been continuously adapted by using IIR filters, as is described in eqIIR and eqIIR2, with $\alpha_{up} = 0.98$. Nevertheless, note that this parameters are not highly influenced by the operating conditions.
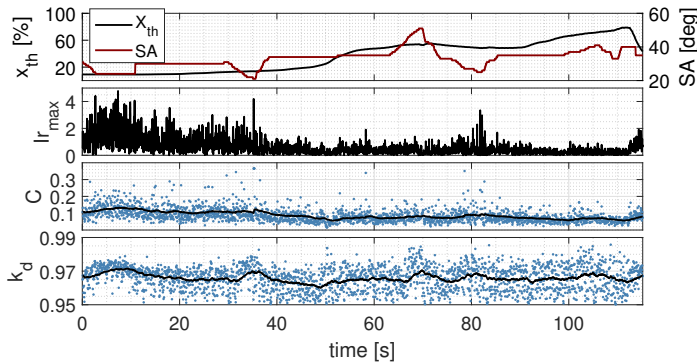

Figure 11: Evolution of model parameters in transient conditions. Engine B.

5.2. Knock recognition: comparison with MAPO

Figure 12 shows E_a and E_c in 1000 cycles at steady state operation for Engine B, where SA was varied from 25 to 40 CAD before TDC. The dashed red line shown on the left plot represents the knocking criteria ($E_c(\theta_2) < E_a(\theta_2)$). Black dots highlights cycles with a knocking criteria of MAPO > 0.6 bar, red crosses highlight cycles with MAPO > 1 bar. In blue circles three different cycles have

been highlighted, the HRR and p_{hp} of these blue circles cycles are represented in the right side to illustrate the advantage of the new knock definition. Both, points 1 and 2, are normal combustion cycles, but are classified as knocking for a MAPO threshold of 0.6 bar, while are no classified as knocking for the knock recognition method proposed. On the other hand, point number 3, which is not detected by MAPO threshold of 0.6 bar, is detected by the method proposed.
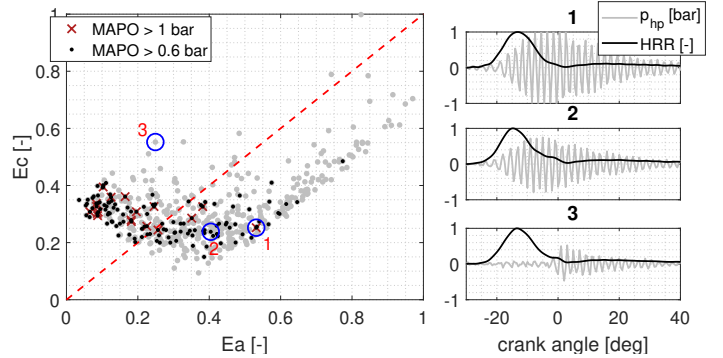

Figure 12: Left plot : E_a and E_c for SA settings from 25 to 40 CAD before TDC. Right plot: Detailed points. Engine B, operation point 2500 RPM. $P_{int} = 1.8$ bar .

The same analysis was performed for engine A at various steps of SA: the classical knock identification method was compared with the new knock criteria. Figure 13 (left plot) compares the percentage of knocking cycles obtained from various levels of MAPO and for the current methodology proposed at each data set. The low threshold chosen, 0.25 bar, has several erratic identifications of knock at no-knocking conditions(SA<=8), while the second threshold, 0.4 bar, which is more representative of an ECU calibration, can only detect part of the cycles that are detected with the proposed methodology. Right plot of Figure 13 shows the knock probability of the new knock event definition versus the knock probability obtained by the MAPO definition with a threshold at 0.4 bar. Note that the new definition is capable of recognizing low-knocking cycles, being the knock probability greater for each SA. The low intensity knocking are, where SI engines use to be controlled has been zoomed in a small plot at the right side, here, it can be seen that a probability of 1 % with a MAPO threshold of 0.4 bar, is equivalent to a knock probability of 8 % of the new method. This higher rate of low-knocking cycles recognition will allow to improve the control in such situations.

Two of the main problems of MAPO are:

1. Difficulty to discern normal combustion from knocking combustion when resonance is heavily excited as in new combustion modes. This issue, which precludes the application of a MAPO criteria in new combustion modes, is solved by the proposed shape
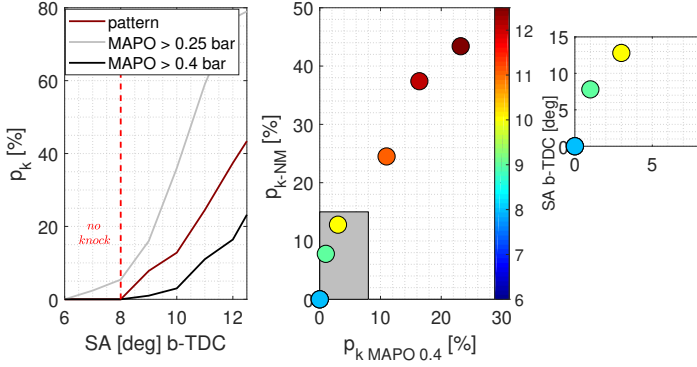
9

Figure 13: Left plot: Knock event probability for different SA steps. Right plot: Knock probability with MAPO threshold 0.4 bar compared with new recognition method. Engine A, operation point 2000 RPM. $P_{int} = 1$ bar.

criteria, as it identifies how is the source of excitation, regardless of the intensity of the fluctuation.

2. Difficulty in recognition low knocking cycles without false recognition in SI engines. This is solved by being able to detect where resonance is excited by the proposed shape criteria, being able to control knock at higher rates

Indeed, the proposed knock recognition method has been implemented in real time with a conventional knock controller. This controller is characterized by adjusting the spark angle $SA_{(i+1)}$ of the forthcoming cycle according to the outcome of the previous firing as:

$$SA_{conv}^i = \begin{cases} SA_{conv}^{i-1} - K_{ret} & if \quad Knock \\ SA_{conv}^{i-1} + K_{adv} & otherwise \end{cases} \quad (15)$$

where i denotes the cycle number, and K_{adv}, K_{ret} are controller gains. K_{ret} is much larger than K_{adv} so the spark slowly advances during non-knocking periods, but it is rapidly retarded if a knock event occurs. These two gains are related by the knock probability, as following:

$$K_{ret} = \frac{1-p}{p} K_{adv} \quad (16)$$

the value of K_{adv} characterize the time response of the controller: on the one hand, high values might allow the controller to reach the optimal value faster when its far from it, but on the other hand the variation of the SA will be higher and hence, higher knock intensities are also expected.

For validation purposes, engine A described in section 2 was tested with a conventional knock controller for MAPO definition (threshold 0.4 bar) and the new recognition method proposed (NM). Knock probability rate was set to 1 % for MAPO definition and 8 % for NM, as figure 13 proves both values to be equivalent. Figure 14 illustrate the controller performance while table 4 summarizes the characteristics of both controllers and the results obtained in terms of IMEP, MAPO and SA. Two tests with

two controller speeds, defined by the K_{adv}, where tested, keeping the engine speed and the injected fuel quantity constant.
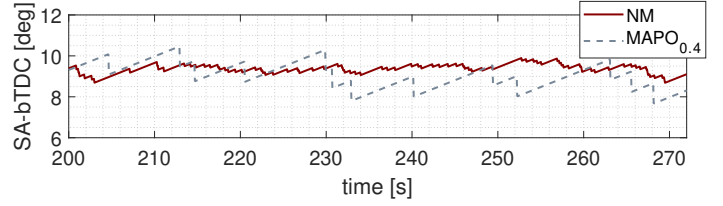

Figure 14: Conventional controller output using both definitions Test 1. Engine A

Table 4: Results of tests performed with conventional knock control. Engine A

	MAPO 0.4 bar		NM	
	$Test_1$	$Test_2$	$Test_1$	$Test_2$
$Time[s]$	600	800	600	800
$K_{adv}[CAD]$	0.01	0.02	0.01	0.02
$p[\%]$	1	1	8	8
$K_{ret}[CAD]$	0.99	1.98	0.115	0.23
$SA_{mean}[deg]$	8.82	8.84	9.3	9.47
$SA_{max}[deg]$	10.84	10.82	9.88	9.9
σ_{SA}	0.57	0.97	0.2	0.3
$IMEP_{mean}[bar]$	11.4	11.58	11.62	10.78
$IMEP_{std}[bar]$	0.15	0.16	0.1	0.11
$MAPO_{max}[bar]$	0.95	0.98	0.45	0.57

Results of Table 4 highlights that the new definition offers more information about knock, which is used to improve the controller performance, i.e. it reduces the variability and achieves a more efficient average value. The higher SA variability makes the controller modify the SA to more advanced values leading to dangerous knocking events. The maximum values for the new recognition method were 0.45 bar and 0.57 bar, while the maximum MAPO when using the classical definition were 0.95 bar and 0.98 bar. The lower variability also allows the controller to reach higher SA which leads to a higher indicated efficiency.

6. Conclusions

An analysis of the resonance excitation of two different engines was performed in this paper, a mathematical tool based on resonance theory was used to characterize resonance and build a model capable to distinguish normal combustion from auto ignition. A new knock recognition method was presented by comparing the resonance indicator with combustion and auto ignition models.

10

This methodology, based on the shape of the resonance evolution, and not only its intensity, will permit the recognition of knock in new combustion modes, where the resonance is highly excited by combustion, while it will facilitate the recognition of low-knocking cycles in SI engines. Results shown that using the new knock event definition improves the performances of the conventional controller in terms of dispersion of the spark advance, average indicate mean effective pressure and maximum knock intensity, and improves knock recognition in cases where combustion strongly excites resonance.

A conventional knock control algorithm was used for comparing the new knock recognition method with classical MAPO definition in a commercial SI engine. Results shown that for maintaining a desired knock level, the new knock recognition method is able to increase the average of the spark advance and reduce the SA dispersion in more than 60 %, which implies a significant reduction of the maximum MAPO reached and an increase in the indicated efficiency.

7. Acknowledgments

Appendix A. Appendix

Appendix A.1. Effect of the window

Different Blackmannharris windows were analyzed in order to choose the proper size, in Figure Appendix A.1 the evolution of the resonance computed as trans is shown, by using various windows sizes.
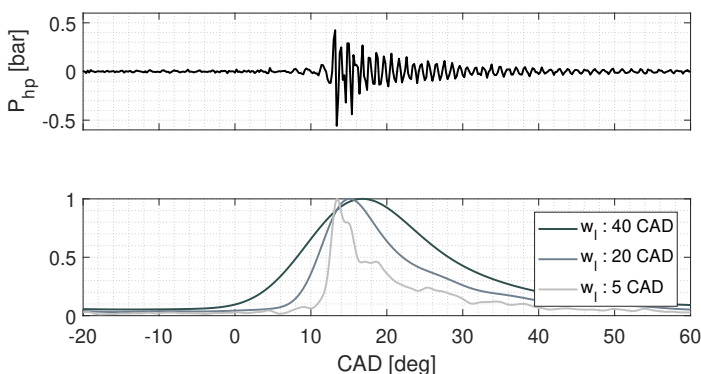

Figure Appendix A.1: Windows size effect in resonance indicator.

A wider window has more resonance information, while a smaller window has less resonance information but more time resolution [37]. Note that a small window has significant noise while a large window cannot precisely appreciate the temporal evolution of the oscillation.

References

[1] Zhen X, Wang Y, Xu S et al. The engine knock analysis–an overview. *Applied Energy* 2012; 92: 628–636.

[2] Guardiola C, Pla B, Bares P et al. An analysis of the in-cylinder pressure resonance excitation in internal combustion engines. *Applied Energy* 2018; 228: 1272–1279.

[3] Netzer C, Seidel L, Ravet F et al. Assessment of the validity of rans knock prediction using the resonance theory. *International Journal of Engine Research* 2020; 21(4): 610–621.

[4] Gholamisheeri M, Givler S and Toulson E. Large eddy simulation of a homogeneously charged turbulent jet ignition system. *International Journal of Engine Research* 2019; 20(2): 181–193.

[5] Soltic P, Hilfiker T and Hänggi S. Efficient light-duty engine using turbulent jet ignition of lean methane mixtures. *International Journal of Engine Research* 2019; : 1468087419889833.

[6] Ayala FA and Heywood JB. Lean si engines: the role of combustion variability in defining lean limits. Technical report, SAE Technical Paper, 2007.

[7] Xu G, Kotzagianni M, Kyrtatos P et al. Experimental and numerical investigations of the unscavenged prechamber combustion in a rapid compression and expansion machine under engine-like conditions. *Combustion and Flame* 2019; 204: 68–84.

[8] Pla B, De la Morena J, Bares P et al. Cycle-to-cycle combustion variability modelling in spark ignited engines for control purposes. *International Journal of Engine Research* 2020; 21(8): 1398–1411.

[9] Attard WP, Bassett M, Parsons P et al. A new combustion system achieving high drive cycle fuel economy improvements in a modern vehicle powertrain. Technical report, SAE Technical Paper, 2011.

[10] Benajes J, Novella R, Gomez-Soriano J et al. Evaluation of the passive pre-chamber ignition concept for future high compression ratio turbocharged spark-ignition engines. *Applied Energy* 2019; 248: 576–588.

[11] Desantes JM, Novella R, De La Morena J et al. Achieving ultra-lean combustion using a pre-chamber spark ignition system in a rapid compression-expansion machine. Technical report, SAE Technical Paper, 2019.

[12] Zhang Y, Shen X, Wu Y et al. On-board knock probability map learning–based spark advance control for combustion engines. *International Journal of Engine Research* 2019; 20(10): 1073–1088.

[13] Kiencke U, Nielsen L and KG SV. Automotive control systems for engine, driveline, and vehicle, 2000. *Measurement Science and Technology p* 1828; .

[14] Laganá AA, Lima LL, Justo JF et al. Identification of combustion and detonation in spark ignition engines using ion current signal. *Fuel* 2018; 227: 469–477.

[15] Bi F, Li X, Liu C et al. Knock detection based on the optimized variational mode decomposition. *Measurement* 2019; 140: 1–13.

[16] Bi F, Ma T and Wang X. Development of a novel knock characteristic detection method for gasoline engines based on wavelet-denoising and emd decomposition. *Mechanical Systems and Signal Processing* 2019; 117: 517–536.

[17] Peyton Jones JC, Shayestehmanesh S and Frey J. Parametric modelling of knock intensity data using a dual log-normal model. *International Journal of Engine Research* 2020; 21(6): 1026–1036.

[18] Shu G, Pan J and Wei H. Analysis of onset and severity of knock in si engine based on in-cylinder pressure oscillations. *Applied Thermal Engineering* 2013; 51(1-2): 1297–1306.

[19] Galloni E. Dynamic knock detection and quantification in a spark ignition engine by means of a pressure based method. *Energy conversion and management* 2012; 64: 256–262.

[20] Parra AFS and Torres AGD. Improvement of a knock model for natural gas si engines through heat transfer evaluation. *International Journal on Interactive Design and Manufacturing (IJIDeM)* 2018; 12(4): 1423–1433.

[21] Gerardin RC, Alves MAF, de França Arruda JR et al. Analysis of spark ignition engine knock signals using fourier and

discrete wavelet transform. Technical report, SAE Technical Paper, 2009.

[22] Park ST and Yang J. Engine knock detection based on wavelet transform. In *Proceedings. The 8th Russian-Korean International Symposium on Science and Technology, 2004. KORUS 2004.*, volume 3. IEEE, pp. 80–83.

[23] Peyton Jones JC, Spelina JM and Frey J. Optimizing knock thresholds for improved knock control. *International Journal of Engine Research* 2014; 15(1): 123–132.

[24] Pla B, De La Morena J, Bares P et al. Knock analysis in the crank angle domain for low-knocking cycles detection. Technical report, SAE Technical Paper, 2020.

[25] Bares P, Selmanaj D, Guardiola C et al. A new knock event definition for knock detection and control optimization. *Applied Thermal Engineering* 2018; 131: 80–88.

[26] Attard WP, Blaxill H, Anderson EK et al. Knock limit extension with a gasoline fueled pre-chamber jet igniter in a modern vehicle powertrain. *SAE International Journal of Engines* 2012; 5(3): 1201–1215.

[27] Draper C. The physical effects of detonation in a closed cylindrical chamber. *Twentieth Annual Report* 1935; : 361–376.

[28] Luján JM, Guardiola C, Pla B et al. Estimation of trapped mass by in-cylinder pressure resonance in hcci engines. *Mechanical Systems and Signal Processing* 2016; 66: 862–874.

[29] Lapuerta M, Armas O and Hernández J. Diagnosis of di diesel combustion from in-cylinder pressure signal by estimation of mean thermodynamic properties of the gas. *Applied Thermal Engineering* 1999; 19(5): 513–529.

[30] Scholl D, Davis C, Russ S et al. The volume acoustic modes of spark-ignited internal combustion chambers. *SAE transactions* 1998; : 1379–1386.

[31] Qi Y, He X, Wang Z et al. Frequency domain analysis of knock images. *Measurement Science and Technology* 2014; 25(12): 125001.

[32] Eng J. Characterization of pressure waves in hcci combustion. Technical report, SAE Technical Paper, 2002.

[33] Shen X, Zhang Y and Shen T. Cylinder pressure resonant frequency cyclic estimation-based knock intensity metric in combustion engines. *Applied Thermal Engineering* 2019; 158: 113756.

[34] Broatch A, Guardiola C, Pla B et al. A direct transform for determining the trapped mass on an internal combustion engine based on the in-cylinder pressure resonance phenomenon. *Mechanical Systems and Signal Processing* 2015; 62: 480–489.

[35] Munjal M. Advances in the acoustics of flow ducts and mufflers. *Sadhana* 1990; 15(2): 57.

[36] Rohani S. *Coulson and Richardson's Chemical Engineering: Volume 3B: Process Control*. Butterworth-Heinemann, 2017.

[37] Guardiola C, Pla B, Bares P et al. Integration of intermittent measurement from in-cylinder pressure resonance in a multi-sensor mass flow estimator. *Mechanical Systems and Signal Processing* 2019; 131: 152–165.